Journal of Medicinal Chemistry

pubs.acs.org/jmc

Article

# A Targeted Covalently Activated Chemotherapy Strategy Synergistically Enhances Cytotoxicity of Ibrutinib and Selectivity of Doxorubicin to B-cell Lymphoma Cells

Xinyue Zhao,[#] Naijie Wei,[#] Ziyang Fang, Yingyan Xie, Xiaowen Yan,[*] and Qiuquan Wang

Cite This: *J. Med. Chem.* 2026, 69, 2387−2399

Read Online

ACCESS | Metrics & More | Article Recommendations | Supporting Information

**ABSTRACT:** To address the low cytotoxicity and drug resistance issues of targeted covalent inhibitor (TCI) ibrutinib and severe side effects of chemotherapeutics doxorubicin (DOX), we developed a novel targeted covalently activated chemotherapy strategy. We designed and synthesized a targeted covalently activated chemotherapy drug, **Ibt-DOX**, which features a targeting ligand of ibrutinib, a DOX, an electrophilic warhead $\alpha$-methylated acrylamide ($\alpha$-MAA) and a self-immolative linker p-hydroxybenzyl alcohol. Upon specifically binding to BTK, **Ibt-DOX** inhibits the BTK-mediated BCR signaling, meanwhile releases DOX and induces immunogenic cell death (ICD), ultimately resulting in not only significantly enhanced targeted B-cell lymphoma cells death compared with ibrutinib, but also reduces the toxic side effects of DOX on BTK- cells. Our work offers a novel strategy through leveraging the synergistic effect of targeted covalent inhibition and the high cytotoxicity of chemotherapy drug, which will inspire the development of new targeted covalent chemotherapeutics for different cancers treatment.

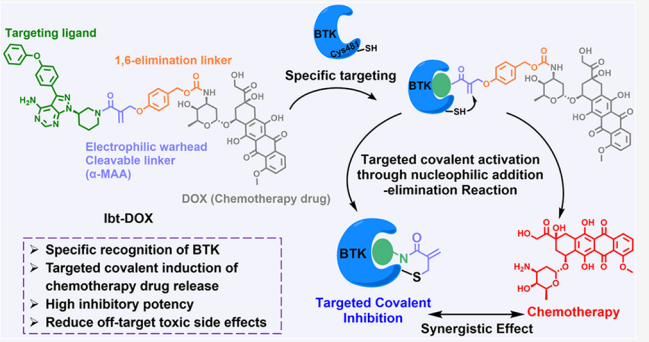




## INTRODUCTION

Targeted Covalent Inhibitors (TCIs) are an important class of pharmacologically active compounds designed to achieve precision therapeutic effects by inhibiting disease-associated proteins through target recognition and covalent bond formation.[1,2] Their action hinges on two discrete steps. First, the high-affinity ligands of TCIs reversibly bind to their biological targets, bringing the weakly electrophilic functional group ("electrophilic warhead") on the ligand into proximity with an appropriately positioned nucleophilic residue (for example, the -SH group of cysteine, the -$NH_2$ group of lysine, the −OH group of tyrosine and serine) on the protein. In the second step, the electrophilic warhead on the ligand and the nucleophilic residue on the protein undergo a spontaneous chemical reaction, generating covalently modified and inactivated proteins.[3,4] U.S. Food and Drug Administration (FDA) has approved numerous targeted covalent inhibitors for cancers treatment.[5,6]

Ibrutinib (also known as PCI-32765), the first TCI of Bruton's tyrosine kinase (BTK), was approved by FDA in 2013 as a breakthrough therapeutic for B-cell malignancies including chronic lymphocytic leukemia (CLL), mantle cell lymphoma (MCL), marginal zone lymphoma (MZL), and Waldenström macroglobulinemia (WM).[7,8] Ibrutinib consists of a specific targeting ligand and an electrophilic warhead (acrylamide). First, the targeting ligand of ibrutinib specifically binds to the ATP-binding pocket of BTK. Subsequently, the acrylamide of ibrutinib spatially approaches the Cys481 residue and forms an irreversible covalent thioether bond through a Michael addition reaction, resulting efficient inhibition of BTK and the B-cell receptor (BCR) signaling pathway, and ultimately inducing apoptosis in B-cell lymphoma cells.[9−11] However, ibrutinib exhibits inferior cytotoxic activity against B-cell malignant cells (Ramos cells ($IC_{50}$ = 14.69 $\mu$M),[12] Raji cells ($IC_{50}$ = 15.99 $\mu$M),[12] OCI-LY10 cells ($IC_{50}$ = 1.72 $\mu$M)[13]). The ibrutinib's low cytotoxicity results in ineffective killing of cancer cells, contributing to drug resistance.[14]

Chemotherapy drugs, the cornerstone drugs for tumor chemotherapy, have dominated the treatment of tumors since the mid-20th century. By directly killing rapidly proliferating cells, chemotherapy drugs, mainly used for broad-spectrum antitumor therapy,[15] include DNA- damaging agents, antimetabolites, microtubule inhibitors, etc. As a representative DNA-damaging agent, doxorubicin (DOX) exerts its effects through DNA insertion and topoisomerase II poisoning.[16,17]

**Received:** August 6, 2025
**Revised:** January 19, 2026
**Accepted:** January 27, 2026
**Published:** January 30, 2026





https://doi.org/10.1021/acs.jmedchem.5c02215
*J. Med. Chem.* 2026, 69, 2387−2399

**Scheme 1. (A) Design of the Targeted Covalently Activated Chemotherapy Drug Ibt-DOX; (B) Proposed Mechanism of Ibt-DOX Activation by BTK via Specific Binding-Triggered Nucleophilic Addition−Elimination Reaction for Targeted Covalent Inhibition and Chemotherapy Drug Releasing**

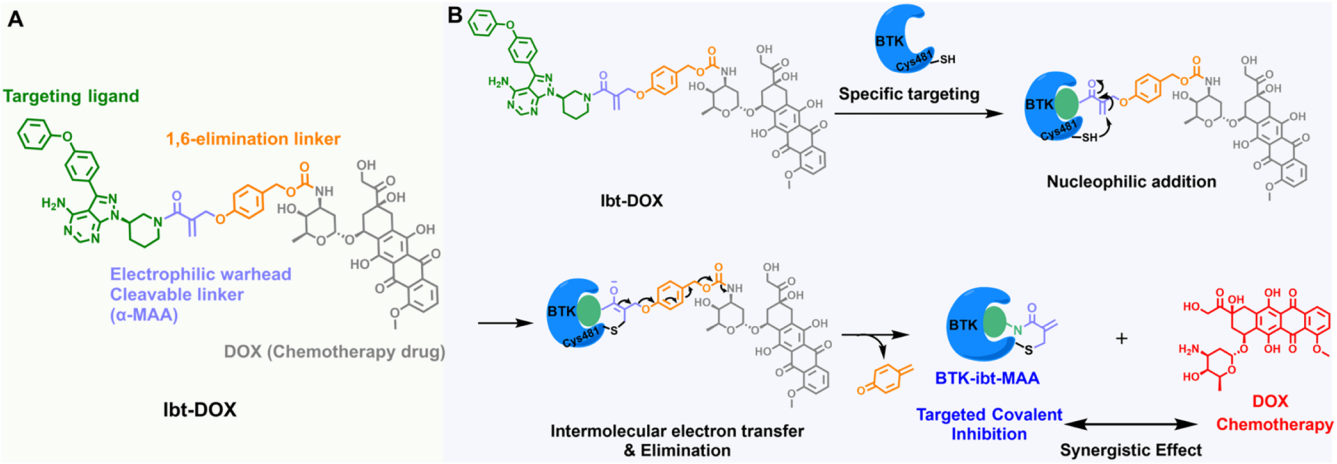


Since approval in 1974, DOX has been the first-line chemotherapy drug for the treatment of tumors such as breast cancer, lymphoma, and sarcoma. Although it shows a significant killing effect on cancer cells, DOX simultaneously damages healthy cells due to the lack of targeted specificity, resulting in serious side effects such as cardiomyopathy, neurotoxicity, myelosuppression, phlebitis and congestive heart failure, which greatly limits its clinical dosage and treatment.[18] Recently, Waring and co-workers developed targeting cytotoxic agents via an addition−elimination mechanism promoted by covalent binding, aiming to address the issue of cytotoxic chemotherapy, i.e., lack of selectivity toward noncancerous cells.[19]

In this study, to enhance the cytotoxicity of ibrutinib and reduce the side effects of DOX, we propose a novel strategy of targeted covalent binding-induced the release of chemotherapy drug to receive an increased therapeutic efficacy and diminished side effects. Based on this strategy, we developed a BTK-targeting and activatable chemotherapy drug (**Ibt-DOX**) to realize the synergistic effect of targeted covalent inhibition and chemotherapy of B-cells lymphoma, which significantly enhanced the cytotoxicity against B-cell Lymphoma cells and reduced the toxic side effects on cells that do not express BTK. **Ibt-DOX** (Scheme 1A), comprises a targeting ligand of ibrutinib as the recognition unit for BTK, a DOX as the releasing chemotherapy drug, an $\alpha$-methylated acrylamide ($\alpha$-MAA)[20,21] group as the electrophilic warhead and a cleavable linker induced by the addition−elimination reaction, and p-hydroxybenzyl alcohol as the self-immolative linker.

As shown in Scheme 1B, upon encountering BTK, the targeting ligand of **Ibt-DOX** interacts specifically with BTK, bringing the $\alpha$-MAA close to Cys481 near the ligand binding site, resulting in a high local concentration. The sulfhydryl group of Cys481 then nucleophilically attacks the C = C bond of $\alpha$-MAA, generating 1,4-addition enol intermediates, in which the elimination reaction occurs owing to intramolecular electron transfer. Generally, the nucleophilic addition−elimination reaction leads to the formation of a covalent bond between $\alpha$-MAA and BTK (BTK-Ibt-MAA), followed by the release of DOX through 1, 6-elimination of p-hydroxybenzyl alcohol.

Based on this novel strategy, targeted covalent inhibition and chemotherapy are realized simultaneously, which synergistically enhance the cytotoxicity of ibrutinib and reduce the side effects of DOX. In addition, the combination of $\alpha$-MAA and p-hydroxybenzyl alcohol linkers enable addition−elimination and self-immolation reactions synchronously, which can be extended to other TCIs and chemotherapy drugs to develop novel targeted covalent chemotherapeutics for different cancers treatment.

## RESULTS AND DISCUSSION

### Design and Synthesis of Ibt-DOX

To realize targeted covalent inhibition and BTK-induced DOX-releasing simultaneously, we planned to connect the targeting ligand of ibrutinib and DOX using $\alpha$-MAA. However, there are multiple hydroxyl groups in DOX, making it difficult to achieve a stoichiometry reaction on a specific hydroxyl group. DOX contains only one amino group, which is an ideal coupling site to control the coupling ratio. However, it is reported that the product formed by coupling amino group with $\alpha$-MAA has a relatively high reactivity with GSH,[21] which is prone to off-target side effects. We thus introduced a p-hydroxybenzyl alcohol to connect the only the -$NH_2$ group of DOX and electrophilic warhead $\alpha$-MAA to reduce the reactivity with GSH, meanwhile without affecting the release of DOX by BTK. The synthesis route of **Ibt-DOX** is shown in Scheme 2A. In acetone, p-hydroxybenzyl alcohol undergoes a substitution reaction with 2-(bromomethyl) acrylic acid in the presence of $K_2CO_3$ to form P-OMAA. P-OMAA, a connecting group between the targeting ligand of ibrutinib and DOX, undergoes an amide condensation reaction with the targeting ligand of ibrutinib to obtain Ibt-MAA−OH. To react with the amino group in DOX, we activated the hydroxyl group of Ibt-MAA−OH with p-nitrophenyl chloroformate to form an amino-reactive intermediate Ibt-MAA-$NO_2$, which finally underwent a substitution reaction with DOX under alkaline conditions to form **Ibt-DOX** (Scheme 2A). Detailed synthetic steps are presented in the Experimental Section, and characterizations of the above compounds by ESIMS and NMR are provided in Figure S1−S10. In order to verify that BTK is covalently bound to the acrylamide of $\alpha$-MAA and thereby induces the release of DOX, we designed and


https://doi.org/10.1021/acs.jmedchem.5c02215
J. Med. Chem. 2026, 69, 2387−2399

Scheme 2. Reagents and Experimental Conditions for the Synthesis of (A) Ibt-DOX and (B) Ibt-PA-DOX[a]

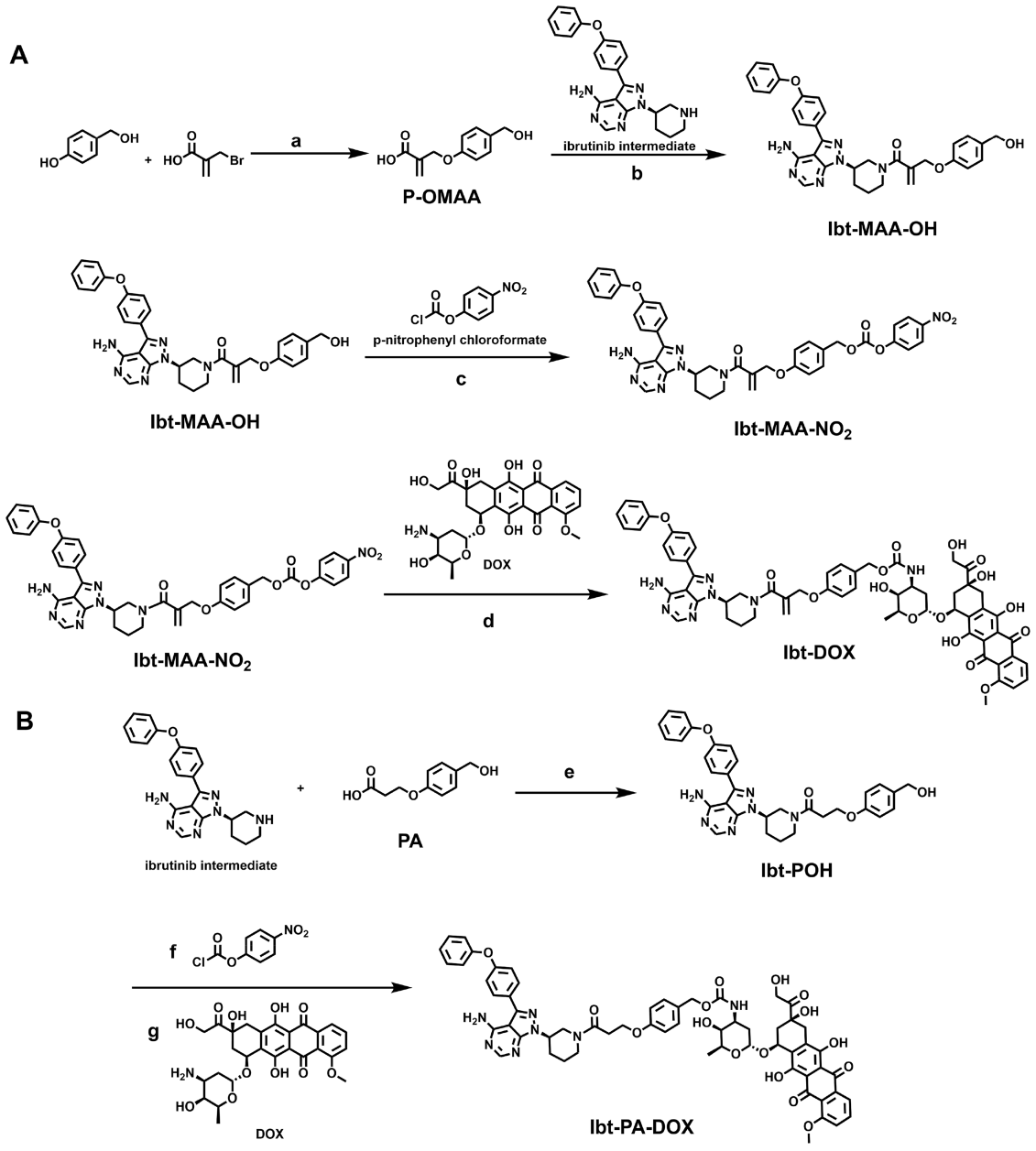


[a](a) $K_2CO_3$, acetone, reflux, 12 h. (b, e) EDC, HOBt, DMF, rt, 4 h. (c, f) pyridine, ice bath, 2 h. (d, g) DIPEA, DMF, rt, 4 h.

synthesized a control compound Ibt-PA-DOX which does not contain the C = C bond of $\alpha$-MAA. The synthesis route of Ibt-PA-DOX is shown in Scheme 2B. The targeting ligand of ibrutinib undergoes an amide condensation reaction with 3-(4-(hydroxymethyl)phenoxy)propanoic acid (PA) to obtain Ibt-POH. In order to react with the amino group in doxorubicin, we activated the hydroxyl group of Ibt-POH by using p-nitrophenyl chloroformate, thereby generating the amino-reactive intermediate. Subsequently, this intermediate undergoes a substitution reaction with DOX, ultimately forming Ibt-PA-DOX. The characterizations of the above compounds by ESIMS and NMR are provided in Figures S11−S16.

## The Inhibitory Efficacy of Ibt-DOX to BTK

We first investigated the affinity of **Ibt-DOX** toward recombinant BTK through a BTK activity inhibition assay using HTRF KinEASE-TK Detection Kit.[13] As shown in Figure 1A,B, the $IC_{50}$ value of ibrutinib was determined to 1.32 nM, consistent with the result reported in the literature.[10] **Ibt-DOX** was found to exhibit inhibitory potency against BTK with an $IC_{50}$ value of 2.89 nM, indicating that the introduction of DOX has a minor impact on the interaction between ibrutinib and BTK. The results demonstrated that **Ibt-DOX** exhibits potent inhibitory activity against BTK. The $IC_{50}$ value of Ibt-PA-DOX was determined to 19.81 nM, demonstrating that the C = C bond of the warhead is important for high affinity binding of Ibt -DOX to BTK.

## Reaction Mechanism of Ibt-DOX toward BTK

To explore the reaction mechanism of **Ibt-DOX** toward BTK, we performed HPLC-ESIMS-based peptide mapping to identify the covalent binding site of BTK labeled by **Ibt-DOX**. The **Ibt-DOX**-labeled BTK for 30 min was subjected to trypsin digestion procedures including protein reduction with


https://doi.org/10.1021/acs.jmedchem.5c02215
J. Med. Chem. 2026, 69, 2387−2399

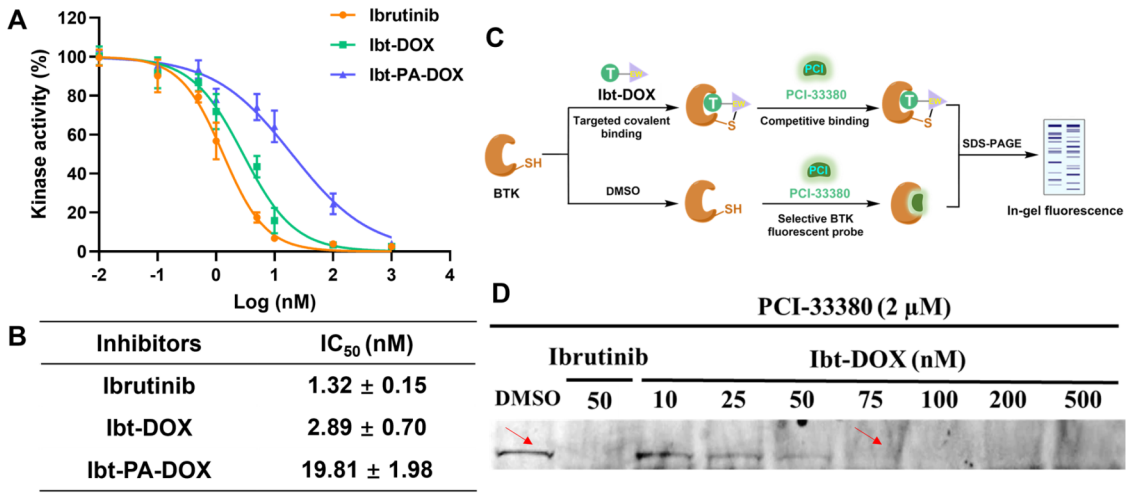


**Figure 1.** (A) Dose−response curves of the activity of recombinant BTK treated with different inhibitors. IC50 values were obtained by fitting the dose−response curves of BTK activity as a function of inhibitors' concentration, data are shown as mean ± SD ($n$ = 3). (B) Table of IC50 values. (C) Schematic illustrating the principle of the competitive binding assay. (D) Concentration-dependent binding of **Ibt-DOX** to BTK in OCI-LY10 cells through the competitive binding assay using PCI-33380.

DTT, iodoacetamide (IAA) alkylation, and trypsin digestion, followed by HPLC-ESIMS-based peptide mapping. MS/MS fragmentation and extracted ion chromatogram of Ibt-MAA-labeled peptide fragment 467−487 (QRPIFIITEYMANGC-(Ibt-MAA)LLNYLR) was detected as shown in Figure S17A,B, the determined molecular weights of which ($[M+3H]^{3+}$, $m/z$, 994.2026; $[M+4H]^{4+}$, $m/z$, 745.9048) are consistent with the calculated ones (calculated $[M+3H]^{3+}$, $m/z$, 994.1680; $[M+4H]^{4+}$ $m/z$, 745.8760) (Figure S17C), indicating that Cys481 is the specific covalent binding site of **Ibt-DOX** on BTK. Iodoacetamide-labeled peptide 467−487 (QRPIFIITEYMANGC(CAM)LLNYLR, calculated $[M+3H]^{3+}$, $m/z$, 862.4431) was not observed in Figure S17B. These results indicate that the reaction between BTK and **Ibt-DOX** was complete within 30 min. Meanwhile, the released DOX ($[M + H]^{+}$ $m/z$, 544.1754) were detected with high intensity, consistent with the calculated $[M + H]^{+}$ $m/z$, 544.1813 (Figure S17D,E). These results demonstrate that the reaction of **Ibt-DOX** with BTK undergoes the nucleophilic addition−elimination reaction pathway. First, the targeting ligand of **Ibt-DOX** interacts with BTK, the sulfhydryl group of Cys481 then nucleophilically attacks the acrylamide of **Ibt-DOX**, which then generate the targeted covalent binding product (BTK-Ibt-MAA), along with the release of DOX.

We also performed HPLC-ESIMS-based peptide mapping to evaluate the reaction products of BTK with Ibt-PA-DOX. The Ibt-PA-DOX ($[M + H]^{+}$ $m/z$, 1134.3637) were detected with high intensity, consistent with the calculated $[M + H]^{+}$ $m/z$, 1134.4091 (Figure S18D,E). Meanwhile, the DOX ($[M + H]^{+}$ $m/z$, 544.1813) were not detected. MS/MS fragmentation and extracted ion chromatogram of IAA-labeled peptide fragment 467−487 (QRPIFIITEYMANGC(IAA)LLNYLR) was detected as shown in Figure S18A,B, the determined molecular weights of which ($[M+2H]^{2+}$, $m/z$, 1293.1225; $[M+3H]^{3+}$, $m/z$, 862.4272) are consistent with the calculated ones (calculated $[M+2H]^{2+}$, $m/z$, 1293.1247; $[M+3H]^{3+}$, $m/z$, 862.4431) (Figure S18C), indicating that Ibt-PA-DOX cannot undergo a covalent binding reaction with BTK and induce the release of DOX. The peptide mapping results demonstrate that the C = C bond of the $\alpha$-MAA warhead plays an important role in both covalent binding with BTK and DOX release.

To clarify the mechanism of **Ibt-DOX** toward BTK in cancer cells (BTK+), we performed HPLC-ESIMS to evaluate the release of DOX by **Ibt-DOX** in OCI-LY10 cells (a human cell line derived from diffuse large B-cell lymphoma, BTK+) and Jurkat cells (human T lymphocyte leukemic cells, BTK-). As shown in Figure S19A, extracted ion chromatogram of the release of DOX was detected in OCI-LY10 cells. The determined molecular weights of DOX ($[M + H]^{+}$, $m/z$, 544.1739) are consistent with the calculated $[M + H]^{+}$, $m/z$, 544.1813 (Figure S19B). However, the DOX were not detected in Jurkat cells. These results demonstrate that **Ibt-DOX** can release free DOX specifically inside BTK+ cancer cells.

Moreover, to explore the reaction of **Ibt-DOX** with GSH, we analyzed the reaction products of **Ibt-DOX** and GSH by HPLC-ESIMS (Figure S20). Ten mM GSH was added to 50 $\mu$M Ibt-DOX (phosphate buffer, pH = 7.4, 100 mM), and HPLC-ESIMS analysis was conducted after different reaction time at 37 °C. As shown in Figure S20, after 8 h' reaction of 10 mM GSH with **Ibt-DOX**, only negligible substitution product (GSH-Ibt-MAA, $[M + H]^{+}$, $m/z$, 760) and released DOX ($[M + H]^{+}$, $m/z$, 544) were detected, indicating the weak reactivity of **Ibt-DOX** with GSH.

## In Situ Reactivity of Ibt-DOX Toward BTK

We further evaluated the reactivity of **Ibt-DOX** with cellular BTK in OCI-LY10 cells through a competitive binding assay employing PCI-33380 (Figure 1C,D, a) Bodipy-modified irreversible BTK probe. After 1-h incubation, PCI-33380 formed stable adducts with cellular BTK (DMSO lane, Figure 1D), and 50 nM ibrutinib achieved full cellular BTK occupancy. Pretreatment of OCI-LY10 cells with **Ibt-DOX** (75 nM) completely eliminated the PCI-33380-labeled BTK band in a concentration-dependent manner. These experimental results indicate that **Ibt-DOX** still maintain the high reactivity with cellular BTK, but its reactivity is lower than that of ibrutinib. We speculate that this phenomenon might be due to the steric hindrance from the appended linker/DOX or reduced electrophilicity as a result of methylation modification at the $\alpha$-position of the acrylamide of ibrutinib.


https://doi.org/10.1021/acs.jmedchem.5c02215
J. Med. Chem. 2026, 69, 2387−2399

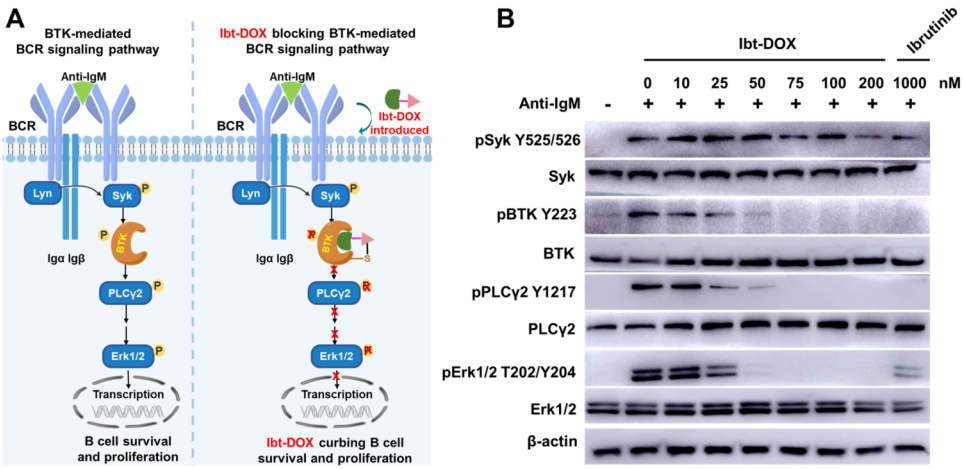


**Figure 2.** (A) Schematic illustrating the BTK-mediated BCR signaling pathway and its inhibition by **Ibt-DOX**. (B) Concentration-dependent inhibition of BCR phosphorylation signaling in OCI-LY10 cells by **Ibt-DOX**, as determined by SDS-PAGE immunoblotting.

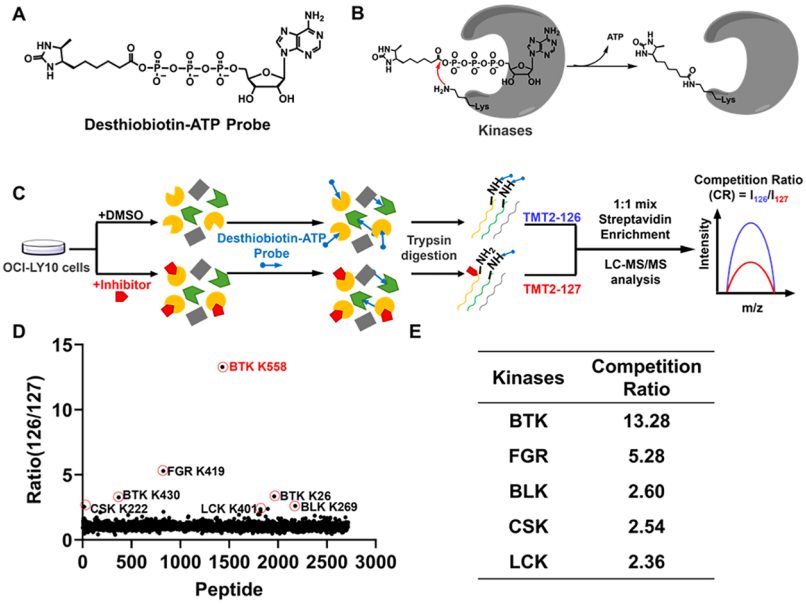


**Figure 3.** (A) Chemical structures of the ActivX Desthiobiotin-ATP Probe (Thermo Scientific). (B) Mechanism of Desthiobiotin-ATP Probe for labeling kinases. (C) The workflow of activity-based protein profiling (ABPP) via LC-MS/MS using a desthiobiotin-ATP probe. (D, E) The competition ratios (CR, $I_{126}/I_{127}$) of kinases in OCI-LY10 cells.

To answer this question, we further designed a control compound Ibt-MAA which contain the targeting ligand and a small $\alpha$-MAA warhead (Figure S21). Characterizations of Ibt-MAA are provided in Figure S22−24. Ibt-MAA−OH (Scheme 2A, Figure S21), whose structure contains one more p-hydroxybenzyl alcohol linker compared with Ibt-MAA, was also used to evaluate the steric hindrance effect. We then investigated the affinity of Ibt-MAA and Ibt-MAA−OH toward recombinant BTK through the BTK activity inhibition assay.[13] The $IC_{50}$ values of Ibt-MAA and Ibt-MAA−OH were determined to 2.03 and 2.13 nM, comparable to that of **Ibt-DOX** (Figure S25A,B). In situ reactivity of Ibt-MAA and Ibt-MAA−OH toward BTK were also evaluated (Figure S25C). By pretreating OCI-LY10 cells with Ibt-MAA (75 nM) and Ibt-MAA−OH (75 nM), the BTK bands labeled by PCI-33380 could be completely eliminated. These results indicate that **Ibt-DOX**, Ibt-MAA and Ibt-MAA−OH exhibit similar reactivity toward BTK, demonstrating that steric hindrance from the appended linker/DOX is not the key reason responsible for the lower reactivity of **Ibt-DOX** compared to that of ibrutinib. As an electron-donating group, the methyl group may increase the electron cloud density of the double bond in the $\alpha$, $\beta$-unsaturated ketone, whose nucleophilic addition reactivity is compromised as a result of the reduced electrophilicity.

We further evaluated the inhibitory effect of **Ibt-DOX** on the BTK-mediated BCR signaling pathway in OCI-LY10 cells by using SDS-PAGE immunoblotting. BTK is a key regulator of the BCR signaling pathway, affecting the proliferation, survival, and other activities of B cells[22] (Figure 2A). We used anti-IgM (a mimic of BCR-antigen) to stimulate the phosphorylation of BTK and its upstream (Syk) and downstream kinases (PLC$\gamma$2, Erk1/2) along the BCR signaling pathway[23] (Figure 2A). As shown in Figure 2B, 75 nM **Ibt-DOX** was found able to completely inhibit the phosphorylation of BTK, as well as its downstream effectors (PLC$\gamma$2, Erk1/2), while the phosphorylation of the upstream kinase Syk was not affected. These


https://doi.org/10.1021/acs.jmedchem.5c02215
J. Med. Chem. 2026, 69, 2387−2399

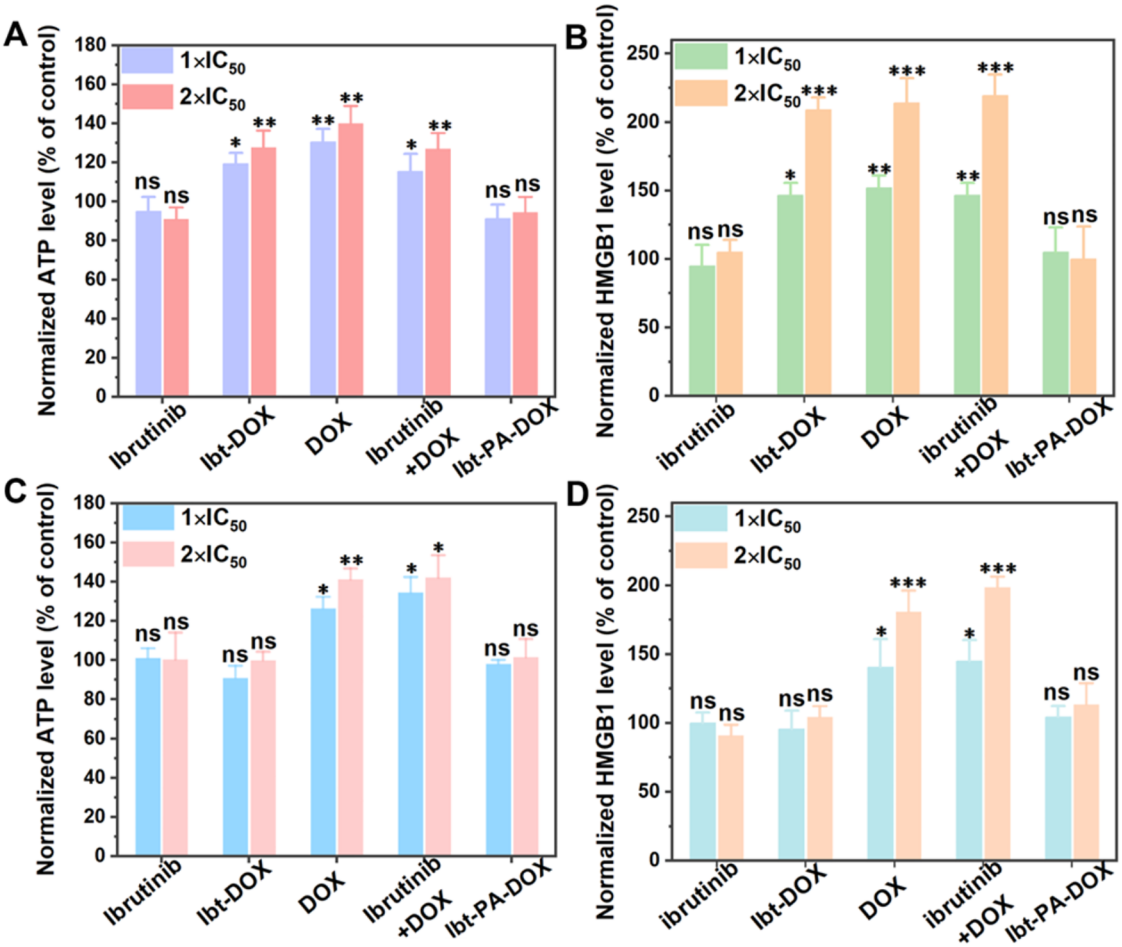


**Figure 4.** Normalized level of extracellular ATP released from OCI-LY10 cells (A) and Jurkat cells (C) after the treatment with inhibitors. The normalized level of extracellular HMGB1 released from OCI-LY10 cells (B) and Jurkat cells (D) after the treatment with inhibitors. Data were normalized to the untreated control, set to 100%, data are shown as mean ± SD ($n$ = 3). Data sets were subjected to statistical analysis using student's $t$ test, and the stars denote the significant difference from the untreated control (*$P$ < 0.05, **$P$ < 0.01, ***$P$ < 0.001, ns, no statistically significant difference).

results indicate that **Ibt-DOX** has a high inhibitory activity on the BTK-mediated BCR signaling pathway.

## In Situ Specificity of Ibt-DOX toward BTK

To explore the specificity of **Ibt-DOX**, we performed activity-based protein profiling (ABPP) via LC-MS/MS using a desthiobiotin-ATP probe (Figure 3A). The desthiobiotin-ATP probe can covalently label conserved lysine residues in or near the ATP-binding pocket of kinases (Figure 3B). To evaluate the selectivity of **Ibt-DOX** toward other kinases, we applied a competitive ABPP strategy to profile the kinase targets of **Ibt-DOX** with this ATP probe.[24−26] The workflow of this strategy is shown in Figure 3C. OCI-LY10 cells were first treated with DMSO or **Ibt-DOX**, then lysed. The cell lysates were labeled by desthiobiotin-ATP probe, subjected to trypsin digestion procedures. Then the peptides were labeled using TMT duplex reagents (TMT2−126/127). The TMT-labeled peptide samples were combined at a 1:1 ratio, enriched by streptavidin magnetic beads and identified and quantified by LC-MS/MS. The in situ selectivity of **Ibt-DOX** toward different kinases was assessed by determining the competition ratios (CR, $I_{126}/I_{127}$).[26,27] As shown in Figure 3D,E, **Ibt-DOX** (1 $\mu$M) exhibited biggest competition ratio with BTK (CR = 13.28), confirming BTK as the primary target. The main off-target kinases were Tyrosine-protein kinase Fgr (FGR), B-lymphoid tyrosine kinase (BLK), Tyrosine-protein kinase CSK (CSK) and Tyrosine-protein kinase Lck (LCK), whose CR values were determined to be 5.28, 2.60, 2.54, 2.36, respectively, obviously lower than the CR of **Ibt-DOX**. Since these off-target kinases have the similar ATP-binding pocket as BTK, and previous studies have shown that ibrutinib also exhibits inhibition activity to BTK ($IC_{50}$ = 0.5 nM), BLK ($IC_{50}$ = 0.5 nM, 1 fold), FGR ($IC_{50}$ = 2.3 nM, 4.6 fold), CSK ($IC_{50}$ = 2.3 nM, 4.6 fold), LCK ($IC_{50}$ = 33.2 nM, 66.4 fold).[10] These results demonstrate that our modification has negligible influence on the selectivity of ibrutinib.

## The ability of Ibt-DOX to Release Damage-Associated Molecular Patterns (DAMPs)

Immunogenic cell death (ICD) is a specific form of regulated cell death that can activate the adaptive immune response in immunocompetent host cells.[28] When cells undergo ICD, dead cells produce new antigenic epitopes and release damage-associated molecular patterns (DAMPs), which can bind, recognize, phagocytose, and present the dead cell antigens to T cells, thereby activating the adaptive immune response and eliminating pathogens or cancer cells.[29] DAMPs include ATP,[30] high-mobility group box 1 protein (HMGB1),[31] and etc. According to the literature, DOX can induce tumor cells to


https://doi.org/10.1021/acs.jmedchem.5c02215
J. Med. Chem. 2026, 69, 2387−2399

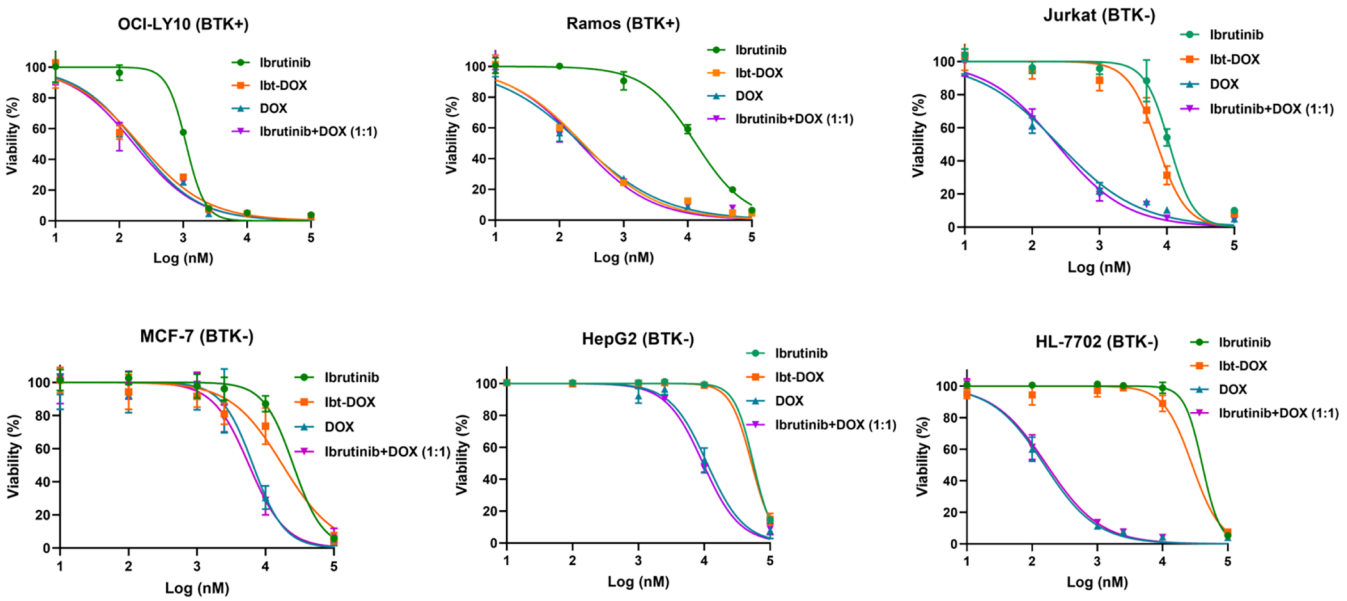


**Figure 5.** Dose−response curves of the viability of cells treated with **Ibt-DOX**, data are shown as mean ± SD ($n$ = 3).

**Table 1. Antiproliferative Activity of Tested Compounds Determined by CCK-8 Assay**[a]

| | $IC_{50}$ ($\mu$M) | | | |
|---|---|---|---|---|
| cells | Ibt-DOX | DOX | ibrutinib | Ibrulinib + Dox (mix 1:1) |
| OCI-LY10 (BTK+) | 0.206 ± 0.01 | 0.191 ± 0.03 | 1.1 ± 0.1 | 0.169 ± 0.02 |
| Ramos (BTK+) | 0.231 ± 0.02 | 0.211 ± 0.03 | 13,5 ± 0.7 | 0.206 ± 0.02 |
| Jurkat (BTK−) | 7.1 ± 0.1 | 0.246 ± 0.02 | 10.8 ± 0.6 | 0.231 ± 0.01 |
| MCF-7 (BTK−) | 17.9 ± 4.4 | 6.5 ± 1.2 | 25,5 ± 2.8 | 5.7 ± 1.7 |
| HepG2 (BTK−) | 52.3 ± 7.8 | 11.1 ± 3.1 | 55.7 ± 6.5 | 9.6 ± 0.4 |
| HL-7702 (BTK−) | 28.4 ± 3.6 | 0.154 ± 0.04 | 40.6 ± 5.9 | 0.168 ± 0.03 |

[a]Cells were treated for 72 h. The data represents the concentration of compounds ($\mu$M) with a 50%-inhibitory effect on cell proliferation. Data are the means ± SD from three independent experiments.

undergo ICD, release DAMPs, and enhance antitumor immune responses.[32,33]

To evaluate the ability of **Ibt-DOX** to release DAMPs in cells, we detected the levels of released HMGB1 and ATP in OCI-LY10 cells (BTK+) and Jurkat cells (BTK-) treated with **Ibt-DOX**. ATP release is another characteristic of ICD and is an important member of the DAMPs family. During the blebbing stage of cell apoptosis, ATP is extruded, usually associated with the autophagy process, mediating the exocytosis of ATP to the extracellular space. CALR belongs to the ″eat me″ signal, ATP is similar to the ″find me″ signal, capable of attracting dendritic cell precursors and activating specific P2 × 7 receptors on dendritic cells (DCs).[34] This activation cascade reaction triggers inflammasomes and stimulates the secretion of interleukins (ILs).[35] As shown in Figure 4A, OCI-LY10 cells were treated with compounds at 1 or 2 times the $IC_{50}$ concentration for 20 h. Compared with the untreated control group, **Ibt-DOX**, Dox, and ibrutinib + Dox groups all led to a significant increase in extracellular ATP release, while the increase in extracellular ATP in cells treated with ibrutinib and Ibt-PA-DOX (noncleavable analog) was negligible. The ATP level in OCI-LY10 cells pretreated with 200 nM and 400 nM **Ibt-DOX** was 20% and 40% higher than that of the control group, respectively. In Jurkat cells, **Ibt-DOX**, ibrutinib and Ibt-PA-DOX could not promote the release of extracellular ATP, while Dox and ibrutinib + Dox groups led to a significant increase in extracellular ATP release. These results indicate that the release of DOX from **Ibt-DOX** is specifically induced by cellular BTK (Figure 4C), and only the released DOX moiety rather than the entire **Ibt-DOX** molecule can promote the release of DAMPs. Together, **Ibt-DOX** (400 nM) is proven to increase the level of extracellular ATP, which is due to the BTK-induced release of DOX from **Ibt-DOX**.

HMGB1 exists in the cell nucleus under nonaging conditions. However, when cells age, it is released from the cell nucleus, and The HMGB1 in the extracellular environment is another related marker of ICD. The release of HMGB1 is usually associated with the late stage of cell apoptosis, at which the cell structure is severely damaged, allowing HMGB1 to pass through the nuclear membrane and the cytoplasmic membrane and be released into the extracellular environment.[36] The HMGB1 released by ICD cells binds to the TLR4 receptor on DCs, promoting DCs activation. Activated DCs will promote the presentation of antigens to T cells.[31] The release of HMGB1 belongs to the latest signal secreted by ICD cells. Hence, we used Enzyme-linked immunosorbent assay (ELISA) to detect the extracellular HMGB1 level after **Ibt-DOX** treatment. OCI-LY10 cells were treated with 1x or 2x $IC_{50}$ for 24 h. The HMGB1 released in the **Ibt-DOX**, Dox, and Ibrutinib + Dox groups was significantly increased (Figure 4B) while ibrutinib and Ibt-PA-DOX could not stimulate the increase of extracellular HMGB1. In Jurkat cells, **Ibt-DOX**, ibrutinib and Ibt-PA-DOX could not promote the increase of


https://doi.org/10.1021/acs.jmedchem.5c02215
J. Med. Chem. 2026, 69, 2387−2399

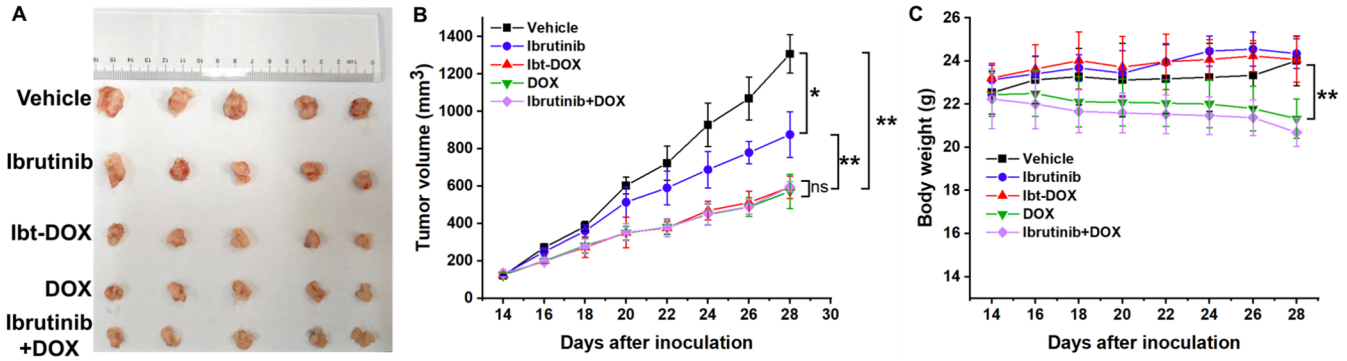


**Figure 6.** In vivo study of the efficacy of **Ibt-DOX**. (A) Photographs of tumors excised from the mice treated with vehicle, ibrutinib, **Ibt-DOX**, DOX or Ibrutinib+DOX for 14 days. (B) Mean volume of xenograft tumor in SCID mice treated with vehicle, ibrutinib, **Ibt-DOX**, DOX or Ibrutinib+DOX. (C) The mice body weights changed over time. Data are shown as mean ± SD ($n$ = 5). Data sets were subjected to statistical analysis using $t$ test, and the stars denote the significant difference from the vehicle (*$P$ < 0.05, **$P$ < 0.01, ns, no statistically significant difference).

extracellular HMGB1 (Figure 4D). The above experiments indicate that **Ibt-DOX** can effectively induce the release of two DAMPs and may induce immunity against tumor cells and participate in tumor destruction due to the BTK-induced release of DOX by **Ibt-DOX**.

### Antiproliferative Activity of Ibt-DOX to Cells

We then evaluated the cytotoxicity of **Ibt-DOX** on cells. We selected OCI-LY10 cells, Ramos cells (human B lymphoma cells, Burkitt lymphoma cells, suspension cells, BTK+) as BTK-positive cells. We chose Jurkat cells (human T lymphocyte leukemic cells, suspension cells, BTK-), HepG2 cells (human liver cancer cell line, adherent cells, BTK-), MCF-7 cells (human breast cancer cell line, adherent cells, BTK-), HL-7702 cells (human hepatocytes, adherent cells, BTK-) as BTK-negative cells. As shown in Figure 5 and Table 1, the $IC_{50}$ values of **Ibt-DOX** for OCI-LY10 cells (BTK+) and Ramos cells (BTK+) were 0.206 $\mu$M and 0.231 $\mu$M, respectively. Compared with the $IC_{50}$ values of the positive drug ibrutinib for OCI-LY10 cells (1.1 $\mu$M) and Ramos cells (13.5 $\mu$M), the cytotoxicity of **Ibt-DOX** on OCI-LY10 cells and Ramos cells were increased by 5.3 and 58.8 times, respectively. The cytotoxicity of **Ibt-DOX** on OCI-LY10 cells and Ramos cells was similar to that of the chemotherapy drug DOX on these two cell lines ($IC_{50(OCI\text{-}LY10)}$ = 0.191 $\mu$M, $IC_{50(Ramos)}$ = 0.211 $\mu$M). Compared with the combination of DOX and ibrutinib ($IC_{50(OCI\text{-}LY10)}$ = 0.169 $\mu$M, $IC_{50(Ramos)}$ = 0.206 $\mu$M), **Ibt-DOX** also had similar cytotoxicity. The above experimental results indicated that the cytotoxicity of **Ibt-DOX** on BTK-expressing cells was significantly increased compared with ibrutinib, and was similar to the cytotoxicity of DOX. The cytotoxicity of **Ibt-DOX** on Jurkat cells, HepG2 cells, MCF-7 cells, and HL-7702 cells were reduced by 28.8, 4.7, 2.7, 184.4 times compared with the DOX treated ones, demonstrating a significantly lower cytotoxicity of **Ibt-DOX** to cells that do not express BTK than that of DOX (Figure 5 and Table 1). All these results indicated that **Ibt-DOX** significantly increased the cytotoxicity of ibrutinib to B-cell lymphoma cells, while reducing the toxic side effects of the broad-spectrum chemotherapy drug DOX to cells that do not express BTK.

### *In Vivo* Antitumor Studies

The high antiproliferative potency of **Ibt-DOX** drove us to study the *in vivo* treatment of SCID mice carrying cancer cells xenograft tumor. We choose OCI-LY10 cells to form mouse xenograft tumors with an initial volume of approximately 100 $mm^3$ for *in vivo* experiments. As shown in Figure 6A,B, the average tumor size after treatment with 2.5 mg/kg **Ibt-DOX** was reduced by 54% compared to the vehicle group at the end of *in vivo* experiments, while the tumor sizes were reduced by 33% in ibrutinib group. These results show a significant antitumor activity of **Ibt-DOX**. Meanwhile, DOX and Ibrutinib +DOX groups exhibit similar antitumor activity. Moreover, after 14 days of treatment, **Ibt-DOX** and ibrutinib treatment did not induce significant body weight change. (Figure 6C) and no poisoning symptom was observed, indicating that **Ibt-DOX** was well-tolerated by SCID mice. However, the mice in DOX and Ibrutinib+DOX groups gained weight loss, indicating the toxic side effects. These results demonstrate that **Ibt-DOX** exhibits not only elevated antiproliferative activities toward lymphoma cells and xenograft tumor compared with ibrutinib, but also reduced toxic side effects than that of DOX.

## CONCLUSIONS

We have established a targeted covalently activated chemotherapy strategy to realize the synergistic effect of targeted covalent inhibition and chemotherapy. We designed and synthesized a novel targeted covalently activated chemotherapy drug, **Ibt-DOX**, by connecting the BTK-targeted covalent ligand with the broad-spectrum chemotherapy drug DOX through $\alpha$-MAA and p-hydroxybenzyl alcohol linkers. **Ibt-DOX** was demonstrated to covalently bind to BTK with high affinity, along with the effective release of DOX. While specifically inhibiting BTK and the BCR signaling pathway, **Ibt-DOX** also releases DAMPs, inducing ICD and inhibiting tumor cell growth. **Ibt-DOX** features not only a significantly enhanced cytotoxicity against B-cell lymphoma cells and mice xenograft tumor compared with ibrutinib, but also reduced toxic side effects of DOX. New targeted covalently activated chemotherapeutics could be developed by reinventing the FDA approved TCIs[5,6] through our strategy for different cancers treatment with high efficacy and low toxic side effects.

## EXPERIMENTAL SECTION

### General Experimental Procedures

2-(Bromomethyl)acrylicacid, 1-hydroxybenzotriazole (HOBt), 1-ethyl-3-(3-dimethyllaminopropyl) carbodiimide hydrochloride (EDC), hydroxybenzyl alcohol, p-nitrophenyl chloroformate, doxorubicin hydrochloride and ibrutinib intermediate 3-(4-phenoxyphenyl)-1-(piperidin-3-yl)-1H-pyrazolo[3,4-$d$]pyrimidin-4-amine were


https://doi.org/10.1021/acs.jmedchem.5c02215
J. Med. Chem. 2026, 69, 2387−2399

purchased from Aladdin (Shanghai, China). PCI-33380 (cat. no. HY-100335) was purchased from TCI. AM-Calcien/PI kit was purchased from Biosharp. BTK recombinant protein (cat. no. 10578-H08B) was purchased from Sino Biological (China). Phospho-Syk (Tyr525/526, cat. no. 2710, Cell signaling), Syk (cat. no. 2712, Cell signaling), Phospho-BTK (Tyr223, cat. no. 5082), BTK (cat. no. 8547), Phospho-PLC$\gamma$2 (Tyr1217, cat. no. 3871), PLC$\gamma$2 (cat. no. 3872), Phospho-p44/42 MAPK (Erk1/2) (Thr202/Tyr204, cat. no. 4370). Erk1/2 (cat. no. 4695) and $\beta$-actin (T202/Y204, cat. no. 4970) were purchased from Cell signaling. Counting Kit-8 (cat. no. C0038), RIPA buffer (cat. no. R0010), ATP Detection Kit (cat. no. S0026) and BCA assay (cat. no. P0012) were purchased from Beyotime. Human HMGB1 ELISA KIT (cat. no. SEKH-0409) was purchased from Solarbio. RPMI 1640 medium (cat. no. 01−100−1A), fetal bovine serum (cat. no. 04-001-1A) and penicillin-streptomycin (cat. no. 03−031−1B) were purchased from Bioind. Pierce Kinase Enrichment Kit with ActivX Desthiobiotin-ATP Probe was purchased from Thermo Fisher.

Nuclear magnetic resonance (NMR) spectra were acquired using a Bruker Avance III 500 MHz spectrometer. High-resolution electrospray ionization time-of-flight mass spectrometry (ESI-TOF-MS) data were acquired using Agilent 6230 mass spectrometer. HPLC-MS analysis was performed using LCMS-2020 (Shimadzu, Japan). Purity analysis was carried out on an LC-20AD analytical HPLC system (Shimadzu, Japan) using an Inertsil ODS-3 C18 column (4.6 I.D. × 150 mm in length, 5 $\mu$m particle size). HPLC analyses confirmed that all inhibitors exhibit purity greater than 95%. Fluorescent gel scanning was visualized by a GE (AI600, USA) scanner (Ex, 460 nm; Em, Cy2 Filter). The peptide mapping data were analyzed using an Ultimate 3000 RSLCnano system coupled to a Bruker Impact II ESI-QTOF-MS equipped with a CaptiveSpray ion source.

## Synthesis of P-OMAA

Hydroxybenzyl alcohol (75 mg, 0.61 mmol), $K_2CO_3$ (250 mg, 1.83 mmol), and 2-(Bromomethyl)acrylic acid (300 mg, 1.83 mmol) were dissolved in acetone (20 mL) and heated under reflux for 12 h. The solvent was removed under reduced pressure to give the crude product **P-OMAA**. HRMS (ESI): $m/z$ Calcd for $C_{11}H_{12}O_4$ $[M\text{-}H]^-$ 207.0736, found 207.0741.

## Synthesis of Compound Ibt-MAA−OH

Compound **P-OMAA** (208 mg, 1.0 mmol) and the intermediate of ibrutinib (425 mg, 1.1 mmol) were dissolved in DMF (10 mL). EDC (230 mg, 1.2 mmol) and HOBt (163 mg, 1.2 mmol) were added. The reaction mixture was stirred at room temperature for 4 h. The crude product was purified by preparative chromatography to afford the white solid **Ibt-MAA−OH**. $^1$H NMR (500 MHz, DMSO-$d_6$) $\delta$ 8.54 (s, 1H), 7.96 −7.84 (m, 1H), 7.69 (t, $J$ = 8.9 Hz, 2H), 7.44 (t, $J$ = 7.8 Hz, 2H), 7.35 (t, $J$ = 10.5 Hz, 1H), 7.28−6.97 (m, 7H), 6.91 (s, 1H), 6.72−6.51 (m, 1H), 5.32 (br. s, 1H), 5.01 (br. s, 1H), 4.51 (m, 2H), 4.26 (m, 1H), 4.12 (q, $J$ = 10.5, 7.8 Hz, 1H), 3.79 (m, 0.5H), 3.73−3.45 (m, 2H), 3.21 (br. s, 0.5H), 2.89 (s, 0.5H), 2.73 (s, 0.5H), 2.23−2.12 (br. s, 1H), 2.06 (s, 1H), 2.01 (m, 1H). $^{13}$C NMR (125 MHz, DMSO) $\delta$ 170.31, 158.20, 157.15, 156.30, 156.17, 155.68, 132.75, 130.11, 128.03, 123.78, 118.98, 114.78, 97.41, 62.80, 60.14, 53.61, 52.47, 52.05, 47.82, 45.61, 43.62, 41.85, 30.94, 29.52, 24.40, 23.37, 22.05, 18.09, 16.72, 13.94, 12.46. HRMS (ESI): $m/z$ Calcd for $C_{33}H_{32}N_6O_4$ $[M + H]^+$ 577.2485, found 577.2409.

## Synthesis of Ibt-MAA-NO$_2$

Compound **Ibt-MAA−OH** (57.7 mg, 0.1 mmol) was dissolved in anhydrous dichloromethane (5 mL). Under an ice bath, pyridine (16 mg, 0.2 mmol) was added dropwise, followed by the addition of p-nitrophenyl chloroformate (24 mg, 0.12 mmol). The mixture was stirred for 2 h at 0 °C. After the reaction was completed as monitored by TLC, the product was purified by column chromatography to yield the white solid compound **Ibt-MAA-NO$_2$**. $^1$H NMR (500 MHz, DMSO-$d_6$) $\delta$ 8.57 (s, 1H), 8.17 (d, $J$ = 8.7 Hz, 2H), 8.09 (d, $J$ = 6.9 Hz, 2H), 7.65 (s, 2H), 7.58 (d, $J$ = 8.4 Hz, 2H), 7.47−7.38 (m, 2H), 7.22−7.05 (m, 5H), 6.95 (d, $J$ = 9.2 Hz, 2H), 6.01 (d, $J$ = 11.5 Hz, 1H), 5.75 (d, $J$ = 22.1 Hz, 1H), 5.44 (s, 1H), 4.89 (s, 1H), 4.63 (s, 2H), 4.29 (s, 0.5H), 4.06 (s, 1H), 3.73 (d, $J$ = 10.8 Hz, 1H), 3.55 (s, 1H), 3.31 (s, 0.5H), 3.08 (s, 0.5H), 2.25 (d, $J$ = 11.1 Hz, 0.5H), 2.15 (s, 2H), 2.06 (s, 2H), 1.89 (s, 0.5H), 1.77 (s, 0.5H). $^{13}$C NMR (125 MHz, DMSO-$d_6$) $\delta$ 164.03, 157.80, 157.60, 156.19, 156.04, 154.91, 149.78, 145.55, 139.55, 132.72, 130.40, 130.16, 128.00, 126.11, 125.50, 123.99, 122.69, 119.16, 118.98, 115.80, 115.34, 114.77, 96.82, 62.77, 53.34, 46.77, 30.94, 29.42, 22.04, 17.97, 16.69, 12.18. HRMS (ESI): calcd for $C_{40}H_{35}N_7O_8$ $[M + H]^+$ 742.2547, found 742.2644.

## Synthesis of Ibt-DOX

Ibt-MAA-NO$_2$ (74.2 mg, 0.1 mmol) and doxorubicin hydrochloride (54.4 mg, 0.1 mmol) were weighed and dissolved in 10 mL DMF. DIPEA (1.2 equiv) was added and the mixture was stirred at room temperature for 4 h. The crude product was purified by preparative chromatography to obtain an orange solid **Ibt-DOX**. $^1$H NMR (500 MHz, DMSO-$d_6$) $\delta$ 13.92 (s, 1H), 13.10 (s, 1H), 8.47 (s, 1H), 8.16 (d, $J$ = 8.7 Hz, 2H), 8.00 (s, 2H), 7.82−7.71 (m, 2H), 7.64 (s, 1H), 7.54 (d, $J$ = 13.3 Hz, 2H), 7.43 (t, $J$ = 7.9 Hz, 2H), 7.19−7.05 (m, 5H), 6.00 (d, $J$ = 20.3 Hz, 1H), 5.75 (d, $J$ = 18.4 Hz, 1H), 5.39 (s, 1H), 5.29 (s, 2H), 4.85 (s, 2H), 4.62 (s, 4H), 4.28 (s, 0.5H), 4.21 (q, $J$ = 6.6 Hz, 1H), 4.13−4.00 (m, 1H), 3.94 (s, 3H), 3.72 (d, $J$ = 10.7 Hz, 1H), 3.63 (s, 1H), 3.55 (s, 1H), 3.39 (s, 1H), 3.31 (s, 0.5H), 3.07 (s, 0.5H), 2.95 (d, $J$ = 18.1 Hz, 1H), 2.75 (d, $J$ = 18.0 Hz, 1H), 2.26 (s, 0.5H), 2.23−2.10 (m, 3H), 2.06 (s, 3H), 1.91 (t, $J$ = 11.1 Hz, 2H), 1.72 (d, $J$ = 7.8 Hz, 1H), 1.17 (d, $J$ = 6.4 Hz, 3H). $^{13}$C NMR (125 MHz, DMSO-$d_6$) $\delta$ 214.07, 206.67, 186.20, 186.09, 176.64, 163.19, 160.71, 158.19, 157.16, 156.31, 156.24, 156.02, 155.67, 154.46, 143.54, 143.42, 136.13, 135.09, 134.43, 134.10, 132.73, 130.13, 130.08, 128.03, 123.80, 119.72, 119.60, 118.99, 118.88, 114.82, 110.53, 110.43, 108.55, 99.24, 97.62, 74.73, 69.54, 66.17, 66.06, 63.89, 62.80, 60.16, 56.55, 53.32, 52.72, 52.01, 46.58, 41.60, 36.17, 31.99, 30.97, 29.46, 28.20, 24.45, 22.07, 21.08, 16.77, 13.96, 12.17. HRMS (ESI): calcd for $C_{61}H_{59}N_7O_{16}$ $[M + H]^+$ 1146.4018 found 1146.4058.

## Synthesis of Compound Ibt-POH

Compound 3-(4-(hydroxymethyl)phenoxy)propanoic acid (**PA**, 196 mg, 1.0 mmol) and the intermediate of ibrutinib (425 mg, 1.1 mmol) were dissolved in DMF (10 mL). EDC (230 mg, 1.2 mmol) and HOBt (163 mg, 1.2 mmol) were added. The reaction mixture was stirred at room temperature for 4 h. The crude product was purified by preparative chromatography to afford the white solid **Ibt-POH**. $^1$H NMR (500 MHz, $CDCl_3$) $\delta$ 8.12 (s, 1H), 7.56 (d, $J$ = 8.5 Hz, 2H), 7.37 (t, $J$ = 7.9 Hz, 2H), 7.23−7.10 (m, 5H), 7.05 (d, $J$ = 7.9 Hz, 2H), 6.80 (d, $J$ = 8.2 Hz, 2H), 6.50 (d, $J$ = 15.0 Hz, 1H), 4.93−4.80 (m, 1H), 4.73 (d, $J$ = 11.0 Hz, 0.5H), 4.53 (s, 2H), 4.28−4.12 (m, 2H), 3.96 (d, $J$ = 13.5 Hz, 0.5H), 3.77−3.64 (m, 0.5H), 3.37 (t, 10.5 Hz, 0.5H), 3.23 (t, 11.5 Hz, 0.5H), 2.93−2.79 (m, 2H), 2.76−2.71 (m, 0.5H), 2.39−2.29 (m, 1H), 2.24 (m, 1H), 2.07−2.02 (m, 0.5H), 1.99−1.94 (m, 0.5H), 1.78−1.66 (m, 1H). $^{13}$C NMR (125 MHz, $CDCl_3$) $\delta$ 169.82, 159.55, 157.90, 155.75, 153.29, 151.48, 146.92, 145.77, 133.38, 130.07, 129.76, 128.63, 125.20, 124.44, 119.17, 114.39, 96.94, 64.43, 64.13, 54.39, 53.34, 49.86, 45.67, 41.93, 32.96, 29.89, 24.71. HRMS (ESI): $m/z$ Calcd for $C_{32}H_{32}N_6O_4$ $[M + H]^+$ 565.2558, found 565.2567.

## Synthesis of Ibt-PA-DOX

Compound **Ibt-POH** (56.5 mg, 0.1 mmol) was dissolved in anhydrous dichloromethane (5 mL). Under an ice bath, pyridine (16 mg, 0.2 mmol) was added dropwise, followed by the addition of p-nitrophenyl chloroformate (24 mg, 0.12 mmol). The mixture was stirred for 2 h at 0 °C. After the reaction was completed as monitored by TLC and concentrated under reduced pressure. Then, active intermediate was dissolved in 10 mL DMF. DIPEA (1.2 equiv) and doxorubicin hydrochloride (54.4 mg, 0.1 mmol) were added and the mixture was stirred at room temperature for 4 h. The crude product was purified by preparative chromatography to obtain an orange solid **Ibt-PA-DOX**. $^1$H NMR (500 MHz, $CDCl_3$) $\delta$ 13.94 (s, 1H), 13.21 (s, 1H), 11.61 (s, 1H), 8.25 (s, 1H), 8.01 (d, $J$ = 7.7 Hz, 1H), 7.77 (t, $J$ = 8.1 Hz, 1H), 7.56 (d, $J$ = 8.2 Hz, 2H), 7.43−7.37 (m, 3H), 7.24−7.05 (m, 7H), 6.82 (d, $J$ = 8.1 Hz, 2H), 6.32 (d, $J$ = 23.3 Hz, 1H), 5.48 (d, $J$ = 3.8 Hz, 1H), 5.27 (s, 2H), 4.94 (s, 2H), 4.75 (s, 2H), 4.55 (d, $J$ =


https://doi.org/10.1021/acs.jmedchem.5c02215
J. Med. Chem. 2026, 69, 2387−2399

13.0 Hz, 0.5H), 4.34 (s, 0.5H), 4.27 (d, $J$ = 12.4 Hz, 1H), 4.20−4.17 (m, 0.5H), 4.16−4.10 (m, 1H), 4.07 (s, 3H), 3.98 (d, $J$ = 13.2 Hz, 0.5H), 3.85−3.76 (m, 1H), 3.65 (s, 1H), 3.37 (t, $J$ = 12.5 Hz, 0.5H), 3.27 (s, 0.5H), 3.23 (s, 1H), 3.02 (d, $J$ = 11.3 Hz, 0.5H), 2.99 (s, 0.5H), 2.97 (s, 0.5H), 2.91 (s, 1H), 2.89−2.85 (m, 1H), 2.76−2.72 (m, 0.5H), 2.37−2.23 (m, 3H), 2.14 (d, $J$ = 14.7 Hz, 1H), 2.07 (d, $J$ = 13.7 Hz, 0.5H), 2.00 (s, 0.5H), 1.85 (d, $J$ = 11.7 Hz, 1H), 1.76 (d, $J$ = 13.4 Hz, 2H), 1.25 (s, 3H). $^{13}$C NMR (125 MHz, $CDCl_3$) $\delta$ 213.96, 187.20, 186.83, 170.70, 169.74, 162.56, 161.21, 160.01, 159.92, 156.32, 155.85, 153.74, 151.70, 147.06, 146.03, 135.92, 135.63, 133.75, 130.26, 130.10, 129.86, 125.40, 125.20, 124.70, 122.38, 121.88, 121.02, 120.05, 119.98, 119.35, 118.63, 114.67, 114.61, 111.73, 111.56, 97.20, 76.75, 69.67, 67.45, 66.67, 65.64, 64.38, 56.82, 53.54, 50.01, 47.13, 45.98, 45.81, 42.05, 37.05, 35.79, 34.12, 33.18, 30.14, 29.82, 24.99, 16.94, 14.24. HRMS (ESI): calcd for $C_{60}H_{59}N_7O_{16}$ $[M + H]^+$ 1134.4091 found 1134.4078.

## Synthesis of Compound Ibt-MAA

Compound 2-(hydroxymethyl)acrylic acid (102 mg, 1.0 mmol) and the intermediate of ibrutinib (425 mg, 1.1 mmol) were dissolved in DMF (10 mL). EDC (230 mg, 1.2 mmol) and HOBt (163 mg, 1.2 mmol) were added. The reaction mixture was stirred at room temperature for 4 h. The crude product was purified by preparative chromatography to afford the white solid **Ibt-MAA**. $^1$H NMR (500 MHz, $CDCl_3$) $\delta$ 8.25 (s, 1H), 7.56 (d, $J$ = 8.6 Hz, 2H), 7.43−7.36 (m, 2H), 7.20 (t, $J$ = 7.4 Hz, 1H), 7.14 (d, $J$ = 8.7 Hz, 2H), 7.08 (d, $J$ = 8.8 Hz, 2H), 5.46 (br. s., 1H), 5.22 (br. s., 1H), 4.91 (m, 1H), 4.61 (s, 1H), 4.31 (br. s., 2H), 4.08 (br. s., 0.5H), 3.70−3.60 (m, 1H), 3.53 (br. s., 0.5H), 3.28 (br. s., 0.5H), 2.84 (br. s., 0.5H), 2.36 (s, 1H), 2.30−2.21 (m, 1H), 2.07−1.95 (m, 1H), 1.75 (s, 1H). $^{13}$C NMR (125 MHz, $CDCl_3$) $\delta$ 170.41, 162.91, 159.87, 155.84, 153.73, 151.67, 147.16, 143.44, 130.23, 129.87, 125.17, 124.68, 120.00, 119.33, 117.09, 115.95, 114.78, 97.24, 65.97, 64.11, 58.50, 30.11, 24.90. HRMS (ESI): calcd for $C_{26}H_{26}N_6O_3$ $[M + H]^+$ 471.2139 found 471.2142.

## HPLC-MS Analysis of the Reaction Products of Ibt-DOX and GSH

The reaction mixture containing **Ibt-DOX** (50 $\mu$M) in potassium phosphate buffer (100 mM, pH 8.0) was incubated with 10 mM GSH at 37 °C, postincubation samples were subjected to analysis using a Shimadzu LCMS-2020 (Shimadzu, Japan).

## HPLC-ESIMS-Based Peptide Mapping Analysis

BTK was labeled with **Ibt-DOX** through a 30 min incubation at room temperature in ammonium bicarbonate buffer (total volume 20 $\mu$L). The reaction mixture consisted of 5 $\mu$L BTK solution (0.48 mg/mL), 1 $\mu$L **Ibt-DOX** (100 $\mu$M in 10% DMSO), and 14 $\mu$L $NH_4HCO_3$ buffer (100 mM, pH 7.4) supplemented with 1 mM $ZnCl_2$ and 1 mM DTT. Following labeling, the protein samples were sequentially processed as follows: reduction with 10 mM DTT at 37 °C for 45 min, alkylation with 40 mM iodoacetamide in the dark at room temperature for 40 min, and digestion with 2 $\mu$L trypsin (Trypsin Gold, NEB #P8101S) for 15 h at 37 °C. The resulting peptides were analyzed using an Ultimate 3000 RSLCnano system coupled to a Bruker Impact II ESI-QTOF-MS equipped with a CaptiveSpray ion source. MS parameters included positive ion polarity, a mass range of 150−2200 $m/z$, Auto MS/MS scan mode, capillary voltage of 1300 V, nanobooster pressure of 0.2 bar, dry gas flow of 3 L/min, and dry temperature of 150 °C.

## Desthiobiotin-ATP Probe Mediated Proteomics Platform

Cell lysates from DMSO-treated (control) and **Ibt-DOX**-exposed groups were diluted with Reaction Buffer to a concentration of 2 mg/mL. Then, 500 $\mu$L (containing 1 mg of protein) of each lysate was transferred to a microcentrifuge tube. To each sample, 10 $\mu$L of $MgCl_2$ (1 M) was added, mixed, and incubated for 1 min at room temperature. Subsequently, the samples were individually incubated with 5 $\mu$M desthiobiotin-ATP probe at room temperature for 30 min. Following probe labeling, proteins were reduced with 10 mM dithiothreitol (DTT) at 37 °C for 1 h and then alkylated with 40 mM iodoacetamide in the dark at room temperature for 30 min. The proteins were precipitated using a methanol/chloroform/water mixture (4:1:3, v/v/v). Briefly, to each 100 $\mu$L sample, 400 $\mu$L of methanol, 100 $\mu$L of chloroform, and 300 $\mu$L of water were added sequentially. The mixture was vortexed thoroughly after each addition. The samples were then centrifuged at 12,000$g$ for 10 min at 4 °C. After centrifugation, the top aqueous layer was carefully removed, and the protein pellet at the interface was washed twice with 500 $\mu$L of methanol. The protein pellets were air-dried and then resolubilized in 500 $\mu$L of 100 mM triethylammonium bicarbonate (TEAB, pH 8.0). The proteins were digested with trypsin at a 1:25 (enzyme-to-protein) ratio overnight at 37 °C in a ThermoMixer (Eppendorf, Germany) with shaking at 1200 rpm.

The resulting peptides were labeled using TMT duplex reagents according to the manufacturer's instructions. Briefly, peptides were labeled with a 1:2 mass ratio (peptides-to-TMT reagents) for 1 h with shaking at 1200 rpm. The reaction was quenched with hydroxylamine (0.3% final concentration) for 15 min at room temperature.

The lightly (TMT2−126, control) and heavily (TMT2−127, **Ibt-DOX**) TMT-labeled peptide samples were combined at a 1:1 ratio. The sample was then subjected to enrichment for desthiobiotin-conjugated peptides using Dynabeads M-280 Streptavidin magnetic beads. Briefly, 50 $\mu$L of streptavidin beads were added to the pooled sample, and the volume was adjusted to 1 mL with PBS. The mixture was incubated with end-overend rotation for 4 h at room temperature.

After enrichment, the beads were collected on a magnetic rack for 3 min. To remove nonspecifically bound peptides, the beads were washed sequentially: twice with 1 mL of PBS containing 0.01% SDS, three times with 1 mL of PBS, and finally five times with 1 mL of water. The enriched peptides were eluted from the beads with 200 $\mu$L of 50% acetonitrile containing 0.1% trifluoroacetic acid, with shaking at 1000 rpm for 10 min at room temperature. This elution step was repeated once, and the combined eluates were dried in a SpeedVac concentrator (Thermo Fisher, U.S.A.). The dried peptides were reconstituted in an aqueous solution of 0.1% formic acid for subsequent LC-MS/MS analysis.

## Mass Spectrometric based ABPP Analysis

Mass spectrometry data were acquired using an Orbitrap Fusion Lumos mass spectrometer coupled to a Proxeon EASY-nLC 1200 LC system (both from Thermo Fisher Scientific). Peptides were separated on a 35 cm long, 100-$\mu$m inner diameter column packed with Accucore resin (2.6 $\mu$m, 150 Å) using a 2.5 h gradient from 4 to 25% acetonitrile in 0.125% formic acid at a flow rate of 525 nL/min. Full MS scans were acquired in the Orbitrap at a resolution of 120,000. The top 10 most intense ions from each MS1 scan were selected for MS2 analysis. MS2 isolation width was set to 0.4 Da, and fragmentation was performed via CID with a normalized collision energy (NCE) of 35%, with analysis in the ion trap. Subsequently, a synchronous precursor selection (SPS) MS3 scan was collected on the top 10 most intense fragment ions from the MS2 spectrum. SPS-MS3 precursors were fragmented by HCD at an NCE of 65% and analyzed in the Orbitrap.

## Data Processing

Mass spectra were processed using a SEQUEST-based software pipeline. Database searches were performed against a custom UniProt Human database (2024 release) containing common contaminants and reversed sequences. Search parameters included: a 50 ppm precursor mass tolerance; a 0.02 Da fragment ion tolerance; full tryptic digestion specificity; static modifications for TMT tags (+229.163 Da) on lysine residues and peptide N-termini, and carbamidomethylation (+57.0214 Da) on cysteine; variable modifications for methionine oxidation (+15.9949 Da) and desthiobiotinylation (+196.1206 Da) on lysine.

Peptide-spectrum matches (PSMs) were filtered to a 1% false discovery rate (FDR) using linear discriminant analysis, which was further propagated to a final protein-level FDR of 1%. For protein quantification, reporter ion intensities from all matching PSMs were summed. The intensity for each reporter ion was extracted from a 0.003 Da window around its theoretical $m/z$ value and corrected for


https://doi.org/10.1021/acs.jmedchem.5c02215
J. Med. Chem. 2026, 69, 2387−2399

isotopic impurities as per the manufacturer's instructions. The signal-to-noise values for each protein were summed across channels and normalized to 100 to obtain relative abundance measurements.

### Intracellular HPLC-MS Analysis

OCI-LY10 cells in the logarithmic growth phase were seeded into 6 cm culture dishes. When the cells reached 80% confluency, they were treated with 25 nM **Ibt-DOX** for 1 h. The cells were then collected, washed three times with PBS, and lysed with 50 $\mu$L methanol to extract intracellular Doxorubicin. Subsequently, the analysis was performed using electrospray ionization quadrupole time-of-flight mass spectrometry (ESI-Q-TOF-MS). The methanolic cell extracts were separated using a high-performance liquid chromatography (HPLC) system (Shimadzu HPLC-20AD, Japan) equipped with an Inertsil ODS-3 C18 column (5 $\mu$m, 4.6 × 150 mm; Shimadzu), which was interfaced online with a Bruker Impact II ESI-Q-TOF-MS.

Chromatographic conditions: The mobile phase consisted of 0.1% formic acid in water (A) and 0.1% formic acid in acetonitrile (B). A gradient elution program was employed as follows: 0−5 min, 98% A; 5−22 min, 98% A to 5% A; 22−27 min, 5% A. The flow rate was set at 1.0 mL/min. Mass spectrometric conditions: Ionization was conducted in positive ion mode. The parameters were set as follows: capillary voltage, 4500 V; end plate offset, 500 V; nebulizer gas pressure, 0.4 bar; dry gas ($N_2$) flow rate, 4.0 L/min; dry gas temperature, 180 °C; mass scan range, $m/z$ 150−1300; spectrum rate, 3 Hz. Additionally, the ion energy for the quadrupole was 4.0 eV, the collision energy in the collision cell was 7.0 eV, the transfer time was 100.0 $\mu$s, and the detector voltage was 2360 V.

### Cell Culture and Cell Viability Assay

Cells were cultured in RPMI 1640 medium supplemented with 10% fetal bovine serum (FBS) under standard humidified conditions (5% $CO_2$, 37 °C). For viability assays, cells were seeded in 96-well plates at a density of 1 × $10^4$ cells per well, incubated for 12 h, and subsequently treated with inhibitors (0.5% DMSO) for 72 h. The medium was removed by centrifugation (1500 rpm, 3 min). Fresh complete medium (100 $\mu$L) and CCK-8 reagent (10 $\mu$L) were sequentially introduced to each well. After a 3-h incubation under physiological conditions, the absorbance in each well was measured at 450 nm using a SpectraMax iD3 microplate reader (Molecular Devices). Each experiment was performed in triplicate. Data were analyzed using GraphPad Prism 8.0 (GraphPad Software).

### BTK Occupancy Assay

For OCI-LY10 cell experiments, 5 × $10^6$ cells were pretreated with varying concentrations of **Ibt-DOX** (0.5% DMSO) for 1 h. After three washes with PBS, the cells were incubated with 2 $\mu$M PCI-33380 for 1 h at room temperature. Subsequently, cells were washed again and lysed in RIPA buffer (4 °C, 30 min). The resulting lysates were clarified by centrifugation (10,000$g$, 8 min, 4 °C) and were quantified using the BCA assay, then subjected to SDS-PAGE followed by fluorescent gel scanning (GE, AI600, USA, Ex, 460 nm; Em, Cy2 Filter).

### BCR Signaling Pathway Inhibition Study

OCI-LY10 cells (5 × $10^6$) were pretreated with graded concentrations of **Ibt-DOX** for 1 h at 37 °C. After thorough washing with PBS, cells were activated with 20 $\mu$g/mL anti-IgM for 10 min at 37 °C. Subsequently, cell lysis was performed using RIPA buffer supplemented with protease/phosphatase inhibitors (4 °C, 30 min). The lysates were clarified by centrifugation (10,000$g$, 8 min, 4 °C) and quantified via BCA assay, then analyzed by Western blot.

### Detection of Extracellular ATP Release

The release of ATP from treated OCI-LY10 and Jurkat cells was detected using an ATP detection kit (Beyotime, S0026). OCI-LY10 cells were seeded in 96-well plates at a density of 2 × $10^4$ cells per well and incubated for 12 h. The medium was then removed by centrifugation (1500 rpm, 4 min), and fresh medium was added. Subsequently, the cells were treated with inhibitors at different concentrations (1× or 2× $IC_{50}$, 72h) in 0.5% DMSO for 20 h. Supernatants from the samples were transferred to the 96-well black plates and analyzed using an ATP bioluminescence assay kit (Beyotime, S0026) according to the manufacturer's instructions. The chemiluminescence intensity of each well was measured using a SpectraMax iD3 microplate reader. Each concentration was repeated three times.

### Detection of Extracellular HMGB1 Protein Release

The extracellular release of HMGB1 protein was detected by ELISA kit (Solarbio, SEKH-0409). OCI-LY10 and Jurkat cells were seeded in 96-well plates at a density of 2 × $10^4$ cells per well, incubated for 12 h, centrifuged (1500 rpm, 4 min) to remove the culture medium, and new culture medium was added. Subsequently, OCI-LY10 and Jurkat cells were treated with inhibitors of different concentrations (1× or 2 × $IC_{50}$,72 h) (0.5% DMSO) for 24 h. After processing is completed, centrifuge at 1500 rpm for 4 min, transfer the cell supernatant to the wells of the ELISA test strip, and follow the manufacturer's instructions for subsequent steps. The absorbance values at wavelengths of 450 and 630 nm were measured using the SpectraMax iD3 microplate reader. All experiments were repeated three times.

### *In Vivo* Efficacy of Ibt-DOX

Female severe combined immunodeficiency disease (SCID) mice were injected subcutaneously with 5 × $10^6$ OCI-LY10 cells. When xenograft tumors' volume reached approximately 100 $mm^3$ that could be clearly observed and measured, mice were randomized into four groups ($n$ = 5/group) and treated with vehicle, ibrutinib, **Ibt-DOX**, DOX and ibrutinib + DOX through tail vein injection once every 2 days (2.5 mg/kg, 0.5% DMSO). Tumor size (tumor volume = length × $width^2$ × 0.52) and body weight were monitored periodically for 14 days. When the tumor volume of the any group reached an intolerable size >2000 $mm^3$, the treatment was ended and the mice were euthanized. All animal experiments were approved by the Xiamen University Laboratory Animal Center (approval code: XMU-LAC20240083), and were performed in accordance with the guidelines of the Xiamen University Institutional Committee for the Care and Use of Laboratory Animals.

## ■ ASSOCIATED CONTENT

### Supporting Information

The Supporting Information is available free of charge at https://pubs.acs.org/doi/10.1021/acs.jmedchem.5c02215.

$^1$H NMR, $^{13}$C NMR, and HRMS spectra of the synthesized compounds, the reaction products of Ibt-DOX with BTK analyzed by HPLC-ESIMS-based peptide mapping, the reaction products of Ibt-PA-DOX with BTK, Ibt-DOX incubating with OCI-LY10 cells, and Ibt-DOX with GSH analyzed by HPLC/ESI-MS, the reactivity of Ibt-MAA, Ibt-MAA−OH toward BTK (PDF)

Molecular formula strings (CSV)

## ■ AUTHOR INFORMATION


### Corresponding Author

**Xiaowen Yan** − *Department of Chemistry and the MOE Key Laboratory of Spectrochemical Analysis & Instrumentation, College of Chemistry and Chemical Engineering, Xiamen University, Xiamen 361005, China; Innovation Laboratory for Sciences and Technologies of Energy Materials of Fujian Province (IKKEM), Xiamen 361005, China;* orcid.org/0000-0001-6608-6044; Email: xwyan@xmu.edu.cn

### Authors

**Xinyue Zhao** − *Department of Chemistry and the MOE Key Laboratory of Spectrochemical Analysis & Instrumentation, College of Chemistry and Chemical Engineering, Xiamen University, Xiamen 361005, China*




https://doi.org/10.1021/acs.jmedchem.5c02215
J. Med. Chem. 2026, 69, 2387−2399

**Naijie Wei** − *Department of Chemistry and the MOE Key Laboratory of Spectrochemical Analysis & Instrumentation, College of Chemistry and Chemical Engineering, Xiamen University, Xiamen 361005, China*

**Ziyang Fang** − *Department of Chemistry and the MOE Key Laboratory of Spectrochemical Analysis & Instrumentation, College of Chemistry and Chemical Engineering, Xiamen University, Xiamen 361005, China*

**Yingyan Xie** − *Department of Chemistry and the MOE Key Laboratory of Spectrochemical Analysis & Instrumentation, College of Chemistry and Chemical Engineering, Xiamen University, Xiamen 361005, China*

**Qiuquan Wang** − *Department of Chemistry and the MOE Key Laboratory of Spectrochemical Analysis & Instrumentation, College of Chemistry and Chemical Engineering, Xiamen University, Xiamen 361005, China;* orcid.org/0000-0002-5166-4048

Complete contact information is available at: https://pubs.acs.org/10.1021/acs.jmedchem.5c02215

## Author Contributions

#X.Z. and N.W. contributed equally. All authors have given approval to the final version ofthe manuscript.

## Notes

The authors declare no competing financial interest.

## ■ ACKNOWLEDGMENTS

This study was financially supported by the National Natural Science Foundation of China (22074127, 22193053), the National Key Research and Development Program of China (2022YFF0710200), the Fujian Provincial Natural Science Foundation of China (2025J01017), the Science and Technology Projects of Innovation Laboratory for Sciences and Technologies of Energy Materials of Fujian Province (IKKEM) (HRTP-[2022]-13), and the Fundamental Research Funds for the Central Universities (20720200073).

## ■ REFERENCES

(1) Singh, J.; Petter, R. C.; Baillie, T. A.; Whitty, A. The resurgence of covalent drugs. *Nat. Rev. Drug Discovery* **2011**, *10*, 307−317.

(2) Lonsdale, R.; Ward, R. A. Structure-based design of targeted covalent inhibitors. *Chem. Soc. Rev.* **2018**, *47*, 3816−3830.

(3) Baillie, T. A. Targeted Covalent Inhibitors for Drug Design. *Angew. Chem., Int. Ed.* **2016**, *55*, 13408−13421.

(4) Ferguson, F. M.; Gray, N. S. Kinase inhibitors: the road ahead. *Nat. Rev. Drug Discovery* **2018**, *17*, 353−377.

(5) Roskoski, R. Properties of FDA-approved small molecule protein kinase inhibitors: A 2025 update. *Pharmacol. Res.* **2025**, *216*, No. 107723.

(6) Roskoski Jr, R. Orally effective FDA-approved protein kinase targeted covalent inhibitors (TCIs): A 2025 update. *Pharmacol. Res.* **2025**, *217*, No. 107805.

(7) Pan, Z.; Scheerens, H.; Li, S.-J.; Schultz, B. E.; Sprengeler, P. A.; Burrill, L. C.; Mendonca, R. V.; Sweeney, M. D.; Scott, K. C. K.; Grothaus, P. G.; Jeffery, D. A.; Spoerke, J. M.; Honigberg, L. A.; Young, P. R.; Dalrymple, S. A.; Palmer, J. T. Discovery of Selective Irreversible Inhibitors for Bruton's Tyrosine Kinase. *ChemMedChem* **2007**, *2*, 58−61.

(8) Wilson, W. H.; Young, R. M.; Schmitz, R.; Yang, Y.; Pittaluga, S.; Wright, G.; Lih, C.-J.; Williams, P. M.; Shaffer, A. L.; Gerecitano, J.; de Vos, S.; Goy, A.; Kenkre, V. P.; Barr, P. M.; Blum, K. A.; Shustov, A.; Advani, R.; Fowler, N. H.; Vose, J. M.; Elstrom, R. L.; et al. Targeting B cell receptor signaling with ibrutinib in diffuse large B cell lymphoma. *Nat. Med.* **2015**, *21*, 922−926.

(9) Ran, F.; Liu, Y.; Wang, C.; Xu, Z.; Zhang, Y.; Liu, Y.; Zhao, G.; Ling, Y. Review of the development of BTK inhibitors in overcoming the clinical limitations of ibrutinib. *Eur. J. Med. Chem.* **2022**, *229*, 114009−114023.

(10) Honigberg, L. A.; Smith, A. M.; Sirisawad, M.; Verner, E.; Loury, D.; Chang, B.; Li, S.; Pan, Z.; Thamm, D. H.; Miller, R. A.; Buggy, J. J. The Bruton tyrosine kinase inhibitor PCI-32765 blocks B-cell activation and is efficacious in models of autoimmune disease and B-cell malignancy. *Proc. Nat. Acad. Sci. U S A* **2010**, *107*, 13075−13080.

(11) Voice, A. T.; Tresadern, G.; Twidale, R. M.; van Vlijmen, H.; Mulholland, A. J. Mechanism of covalent binding of ibrutinib to Bruton's tyrosine kinase revealed by QM/MM calculations. *Chem. Sci.* **2021**, *12*, 5511−5516.

(12) Guo, X.; Yang, D.; Fan, Z.; Zhang, N.; Zhao, B.; Huang, C.; Wang, F.; Ma, R.; Meng, M.; Deng, Y. Discovery and structure-activity relationship of novel diphenylthiazole derivatives as BTK inhibitor with potent activity against B cell lymphoma cell lines. *Eur. J. Med. Chem.* **2019**, *178*, 767−781.

(13) Zhao, Y.; Zhao, X.; Duan, L.; Hou, R.; Gu, Y.; Liu, Z.; Chen, J.; Wu, F.; Yang, L.; Le, X. C.; Wang, Q.; Yan, X. Reinvent Aliphatic Arsenicals as Reversible Covalent Warheads toward Targeted Kinase Inhibition and Non-acute Promyelocytic Leukemia Cancer Treatment. *J. Med. Chem.* **2024**, *67*, 5458−5472.

(14) Shah, B.; Zhao, X.; Silva, A. S.; Shain, K. H.; Tao, J. Resistance to Ibrutinib in B Cell Malignancies: One Size Does Not Fit All. *Trends Cancer* **2018**, *4*, 197−206.

(15) Scott, E. C.; Baines, A. C.; Gong, Y.; Moore, R.; Pamuk, G. E.; Saber, H.; Subedee, A.; Thompson, M. D.; Xiao, W.; Pazdur, R.; Rao, V. A.; Schneider, J.; Beaver, J. A. Trends in the approval of cancer therapies by the FDA in the twenty-first century. *Nat. Rev. Drug Discovery* **2023**, *22*, 625−640.

(16) Nitiss, J. L. Targeting DNA topoisomerase II in cancer chemotherapy. *Nat. Rev. Cancer* **2009**, *9*, 338−350.

(17) DeVita, V. T., Jr.; Chu, E. A History of Cancer Chemotherapy. *Cancer Res.* **2008**, *68*, 8643−8653.

(18) Cheung-Ong, K.; Giaever, G.; Nislow, C. DNA-Damaging Agents in Cancer Chemotherapy: Serendipity and Chemical Biology. *Chem. Biol.* **2013**, *20*, 648−659.

(19) Morese, P. A.; Anthony, N.; Bodnarchuk, M.; Jennings, C.; Martin, M. P.; Noble, R. A.; Phillips, N.; Thomas, H. D.; Wang, L. Z.; Lister, A.; Noble, M. E. M.; Ward, R. A.; Wedge, S. R.; Stewart, H. L.; Waring, M. J. Targeting Cytotoxic Agents through EGFR-Mediated Covalent Binding and Release. *J. Med. Chem.* **2023**, *66*, 12324−12341.

(20) Zhuang, J.; Zhao, B.; Meng, X.; Schiffman, J. D.; Perry, S. L.; Vachet, R. W.; Thayumanavan, S. A programmable chemical switch based on triggerable Michael acceptors. *Chem. Sci.* **2020**, *11*, 2103−2111.

(21) Reddi, R. N.; Resnick, E.; Rogel, A.; Rao, B. V.; Gabizon, R.; Goldenberg, K.; Gurwicz, N.; Zaidman, D.; Plotnikov, A.; Barr, H.; Shulman, Z.; London, N. Tunable Methacrylamides for Covalent Ligand Directed Release Chemistry. *J. Am. Chem. Soc.* **2021**, *143*, 4979−4992.

(22) Pal Singh, S.; Dammeijer, F.; Hendriks, R. W. Role of Bruton's tyrosine kinase in B cells and malignancies. *Mol. Cancer* **2018**, *17*, 57−79.

(23) Woyach, J. A.; Johnson, A. J.; Byrd, J. C. The B-cell receptor signaling pathway as a therapeutic target in CLL. *Blood* **2012**, *120*, 1175−1184.

(24) Patricelli, M. P.; Nomanbhoy, T. K.; Wu, J.; Brown, H.; Zhou, D.; Zhang, J.; Jagannathan, S.; Aban, A.; Okerberg, E.; Herring, C.; Nordin, B.; Weissig, H.; Yang, Q.; Lee, J.-D.; Gray, N. S.; Kozarich, J. W. In Situ Kinase Profiling Reveals Functionally Relevant Properties of Native Kinases. *Chem. Biol.* **2011**, *18*, 699−710.

(25) Worboys, J. D.; Sinclair, J.; Yuan, Y.; Jørgensen, C. Systematic evaluation of quantotypic peptides for targeted analysis of the human kinome. *Nat. Methods* **2014**, *11*, 1041−1044.

(26) Wang, C.; Weerapana, E.; Blewett, M. M.; Cravatt, B. F. A chemoproteomic platform to quantitatively map targets of lipid-derived electrophiles. *Nat. Methods* **2014**, *11*, 79−85.
(27) Kuljanin, M.; Mitchell, D. C.; Schweppe, D. K.; Gikandi, A. S.; Nusinow, D. P.; Bulloch, N. J.; Vinogradova, E. V.; Wilson, D. L.; Kool, E. T.; Mancias, J. D.; Cravatt, B. F.; Gygi, S. P. Reimagining high-throughput profiling of reactive cysteines for cell-based screening of large electrophile libraries. *Nat. Biotechnol.* **2021**, *39*, 630−641.
(28) Kroemer, G.; Galluzzi, L.; Kepp, O.; Zitvogel, L. Immunogenic Cell Death in Cancer Therapy. *Annu. Rev. Immunol.* **2013**, *31*, 51−72.
(29) Krysko, D. V.; Garg, A. D.; Kaczmarek, A.; Krysko, O.; Agostinis, P.; Vandenabeele, P. Immunogenic cell death and DAMPs in cancer therapy. *Nat. Rev. Cancer* **2012**, *12*, 860−875.
(30) Garg, A. D.; Krysko, D. V.; Verfaillie, T.; Kaczmarek, A.; Ferreira, G. B.; Marysael, T.; Rubio, N.; Firczuk, M.; Mathieu, C.; Roebroek, A. J. M.; Annaert, W.; Golab, J.; de Witte, P.; Vandenabeele, P.; Agostinis, P. A novel pathway combining calreticulin exposure and ATP secretion in immunogenic cancer cell death. *EMBO J.* **2012**, *31*, 1062−1079.
(31) Apetoh, L.; Ghiringhelli, F.; Tesniere, A.; Obeid, M.; Ortiz, C.; Criollo, A.; Mignot, G.; Maiuri, M. C.; Ullrich, E.; Saulnier, P.; Yang, H.; Amigorena, S.; Ryffel, B.; Barrat, F. J.; Saftig, P.; Levi, F.; Lidereau, R.; Nogues, C.; Mira, J.-P.; Chompret, A.; et al. Toll-like receptor 4−dependent contribution of the immune system to anticancer chemotherapy and radiotherapy. *Nat. Med.* **2007**, *13*, 1050−1059.
(32) Galluzzi, L.; Buqué, A.; Kepp, O.; Zitvogel, L.; Kroemer, G. Immunosuppressive cell death in cancer. *Nat. Rev. Immunol.* **2017**, *17*, 402.
(33) Sarkar, A.; Novohradsky, V.; Maji, M.; Babu, T.; Markova, L.; Kostrhunova, H.; Kasparkova, J.; Gandin, V.; Brabec, V.; Gibson, D. Multitargeting Prodrugs that Release Oxaliplatin, Doxorubicin and Gemcitabine are Potent Inhibitors of Tumor Growth and Effective Inducers of Immunogenic Cell Death. *Angew. Chem., Int. Ed.* **2023**, *62*, No. e202310774.
(34) Michaud, M.; Martins, I.; Sukkurwala, A. Q.; Adjemian, S.; Ma, Y.; Pellegatti, P.; Shen, S.; Kepp, O.; Scoazec, M.; Mignot, G.; Rello-Varona, S.; Tailler, M.; Menger, L.; Vacchelli, E.; Galluzzi, L.; Ghiringhelli, F.; di Virgilio, F.; Zitvogel, L.; Kroemer, G. Autophagy-Dependent Anticancer Immune Responses Induced by Chemotherapeutic Agents in Mice. *Science* **2011**, *334*, 1573−1577.
(35) Ghiringhelli, F.; Apetoh, L.; Tesniere, A.; Aymeric, L.; Ma, Y.; Ortiz, C.; Vermaelen, K.; Panaretakis, T.; Mignot, G.; Ullrich, E.; Perfettini, J.-L.; Schlemmer, F.; Tasdemir, E.; Uhl, M.; Génin, P.; Civas, A.; Ryffel, B.; Kanellopoulos, J.; Tschopp, J.; André, F.; et al. Activation of the NLRP3 inflammasome in dendritic cells induces IL-1$\beta$−dependent adaptive immunity against tumors. *Nat. Med.* **2009**, *15*, 1170−1178.
(36) Bell, C. W.; Jiang, W.; Reich, C. F., 3rd; Pisetsky, D. S. The extracellular release of HMGB1 during apoptotic cell death. *Am. J. Physiol. Cell Physiol.* **2006**, *291*, C1318−1325.




https://doi.org/10.1021/acs.jmedchem.5c02215
J. Med. Chem. 2026, 69, 2387−2399